Accepted manuscript. Published in Géotechnique (2019). Version of record: https://doi.org/10.1680/jgeot.17.P.299. This is the authors' final version after peer review. Please cite the published article.

Grain size and time effect on the deformation of rockfill dams: a case study on the Shuibuya CFRD

Xiang Zhou[1], Gang Ma[2], Yida Zhang[1*]

ABSTRACT

The mechanical behaviour of coarse granular materials critically depends on their grain size distributions. In settlement analysis of rockfill dams, however, the stress-strain curves obtained from specimens with reduced gradations are often used to approximate the behaviour of prototype rockfills. Accumulated evidence has shown that such practice can underestimate the settlement of concrete face rockfill dams (CFRDs), leading to unexpected damage of the concrete slabs and excessive leakage of the dam. In this paper, the recently developed rate-dependent breakage mechanics theory and breakage-energy scaling law is applied for the settlement analysis of the Shuibuya CFRD. The model is firstly calibrated using results from triaxial test on reduced specimens and then extrapolated to represent the behaviour of prototype rockfills. The constitutive equations are implemented in a finite element package and later applied to full-scale simulations of the dam covering its construction, impoundment and operation phases. The predicted settlement profiles agree reasonably well with the data measured from the internal displacement gauges, thus corroborating the predictive capability of the new methodology. Finally, it is shown that neglecting the scaling and creep effect in the constitutive behaviour of rockfills will underestimate the maximum settlement of the dam by 14% and 18%, respectively.

[1] University of Colorado Boulder, Department of Civil, Environmental and Architectural Engineering, Boulder, CO, USA
[2] State Key laboratory of Water Resources and Hydropower Engineering Science, Wuhan University, Hubei Province, China

1 INTRODUCTION

Accurate prediction of the settlement of rockfill dams is hindered by several uncertainties: (1) rockfills used in dam construction are often provided by local coarse gravelly deposits, rock quarries or excavations, which can have a variety of geological origins (e.g. schist, greywacke, slate) and grain sizes (e.g. maximum grain size D_{max} varies between 200~1000 mm) (Naylor et al., 1986; Alonso et al., 2011); (2) the internal stress of high dams can be as high as several megapascals lasting for its entire service time (Wen et al., 2017), during which the time-dependent behaviour of rockfills becomes important. Obtaining the mechanical behaviour of such a variety of rockfills at extended time scales is difficult given the spatial and temporal limitations of laboratory testing programs. The largest specimen that can be accommodated by large-scale triaxial devices is 1.13 m in diameter and 2.5 m in height, which corresponds to a D_{max} of 180 mm (Marsal, 1973; Marsal, 1967). The common diameters for the rockfill specimens are limited to under 1m and thus require even smaller D_{max} (Marachi et al., 1972; Ovalle et al., 2014; Chávez et al., 2009). This implies that rockfill specimens with reduced grain sizes have to be used to infer the properties of the prototype materials. Creep tests typically last for several months (Cheng and Ding, 2004), which prohibits a systematic characterization of their time-dependent responses prior to dam construction. For these reasons, grain size effect is routinely neglected in the settlement prediction of CFRDs, assuming that the parameters calibrated from reduced specimens are representative of the original rockfills. Creep is sometimes considered in the finite element (FE) analyses using empirical models with 7 to 9 parameters (Zhou et al., 2010; Pramthawee et al., 2017) that can be only determined through back analysis. These simplifications and uncertainties have generally lead to an underestimated settlement of large CFRDs. For example, at the design stage of the Shuibuya CFRD, the predicted maximum settlement 1.36~1.92 m is significantly lower than the observed 2.5 m after three years of operation. Such underprediction cannot be fixed by considering creep, which gives a maximum settlement of 2.05~2.38m. Other examples are listed in Table 1 (Zhu et al.,

2009). These underestimations have led to unconservative design of concrete slabs, thus increasing the risk of face cracking, dam leakage and damage of the affiliated infrastructures (e.g. crest highways).

Table 1: Examples of CFRD that have experienced excessive settlement

Name	Height (m)	Complete	Maximum vertical settlement (m)	
			Predicted	Measured (time, yr)
Tianshengqiao-I	178	1998	1.24~2.05	3.47 (2000)
Hongjiadu	179.5	2005	0.76	1.42 (2009)
Sanbanxi	185.5	2006	0.8	1.56 (2006)
Shuibuya	233	2006	1.36~1.92	2.5 (2009)

This paper presents a strategy to incorporate the grain size and time effects in modelling rockfill dams and examine its predictive capability through a comprehensive case study. Specifically, we integrate the rate-dependent breakage mechanics model recently developed by Zhang and Buscarnera (2017) with the breakage-energy scaling law proposed by Zhang et al. (2016) to formulate a new strategy for continuum-based settlement assessment of rockfill structures (section 2). This model is uniquely equipped to study the scale and time effect in rockfill structures for the following reasons: 1) all of the model parameters have clear physical meanings and well-defined calibration procedures, which permits forward predictions of settlement based only on laboratory tests prior to dam construction; 2) The scaling relation for this model has been thoroughly studied using existing datasets (Zhang and Buscarnera, 2014), fracture-mechanics analysis at grain scale (Zhang et al., 2016), Discrete Element Method (DEM) modelling (Cil and Buscarnera, 2016) and micro-macro experiments (Sohn et al., 2017), which permits a rational incorporation of the scaling effect in rockfill engineering. The performance of this framework is evaluated through a case study on the Shuibuya dam (Hubei, China), currently the tallest CFRD in the world (Section 3). This dam is heavily instrumented with settlement monitoring systems and the rockfills have been well characterized by large-scale triaxial tests, providing sufficient data for the calibration and benchmarking of the proposed framework. The constitutive model is implemented in a FE code and a FE mesh is constructed for the

Shuibuya dam (section 4). Predictive exercises and parametric studies are conducted to elucidate the impact of scaling and time on the deformation of CFRDs (sections 5 and 6).

2 THEORY

2.1 Rate-dependent breakage mechanics

The rate-dependent breakage mechanics is an extension of the original theory by Einav (2007a; 2007b) to model the instantaneous and delayed crushing of granular materials and the accompanied development of inelastic strains. Following the Hyperplasticity formalism (Houlsby and Puzrin, 2007), the model can be summarized by two scalar functions:

$$\Psi\left(\varepsilon_{ij}^{e}, B\right)=\frac{1}{2}\left(1-\vartheta B\right)\left(K\varepsilon_{v}^{e2}+3G\varepsilon_{s}^{e2}\right) \tag{1}$$

$$w\left(\overline{E}_{B}, \overline{\sigma}_{ij}, B\right)=\frac{E_{c}\dot{B}_{0}}{2\left(1-B\right)^{2}}\frac{\overline{\varsigma}_{pB}^{n/2+1}}{n/2+1} \tag{2}$$

where Ψ is the Helmholtz free energy and w is the flow potential; $\overline{\varsigma}_{pB}\left(\overline{E}_{B}, \overline{\sigma}_{ij}\right)=\left\langle \overline{y}_{pB}\left(\overline{E}_{B}, \overline{\sigma}_{ij}\right)\right\rangle$ is the breakage overstress function that measures the distance from the current stress state to the yield surface $\overline{y}_{pB}$ in dissipative stress space; $\langle\cdot\rangle$ is the Macaulay bracket; $\overline{E}_{B}$ and $\overline{\sigma}_{ij}$ are dissipative stresses; superscript 'e' denotes the elastic component; $\varepsilon_{v}=\varepsilon_{ii}$ and $\varepsilon_{s}=\sqrt{\frac{2}{3}e_{ij}e_{ij}}$ are the volumetric and deviatoric strains respectively; ε_{ij} and $e_{ij}=\varepsilon_{ij}-\frac{1}{3}\varepsilon_{v}\delta_{ij}$ are the strain tensor and its deviator respectively; B is the Einav's breakage index serving as an internal state variable in the model (i.e. B=0 for uncrushed state and B=1 for completely crushed state); ϑ is the grading index; K and G are the bulk and shear modulus; E_c is the critical breakage energy, the physical meaning of which will be further discussed in the next section; $\dot{B}_0$ is a fluidity parameter (inverse of viscosity); n is the corrosion index that characterize microscopically the stress-dependency of crack velocity in rock minerals (Atkinson, 1982; Oldecop and Alonso, 2007). Applying hyperelastic relations, equation (1) leads to an isotropic linear elastic model:

$$\sigma_{ij} = \frac{\partial \Psi}{\partial \varepsilon_{ij}^e} = \frac{\partial \Psi}{\partial \varepsilon_v^e}\frac{\partial \varepsilon_v^e}{\partial \varepsilon_{ij}^e} + \frac{\partial \Psi}{\partial \varepsilon_s^e}\frac{\partial \varepsilon_s^e}{\partial \varepsilon_{ij}^e} = \left(1-\vartheta B\right)\left(K\varepsilon_v^e\delta_{ij} + 2Ge_{ij}^e\right) \tag{3}$$

$$E_B = -\frac{\partial \Psi}{\partial B} = \frac{1}{2}\vartheta\left(K\varepsilon_v^{e2} + 3G\varepsilon_s^{e2}\right) \tag{4}$$

where E_B is the breakage energy quantifying the release of the stored energy upon the evolution of GSD of the granular system. The flow potential equation (2) defines the inelastic response of the system and represents a major deviation from the original breakage mechanics theory. Firstly, it corresponds to a non-homogenous dissipation rate function which permits a rate-dependent growth of the internal variables (i.e. $B, \varepsilon_v^p, \varepsilon_s^p$) as opposite to first-order homogenous dissipation functions used in rate-independent hyperplastic models (Collins and Houlsby, 1997; Houlsby, 2014). Secondly, the breakage evolution law is motivated from the kinetics of fracture growth at grain scale rather than assumed a priori from curve-fitting exercises. The hypothesis is that the creep of granular matrix subjected to high confining stresses is a smeared outcome of consecutive grain breakage events due to time-dependent fracture growth within particles (Figure 1, more details can be found in Zhang and Buscarnera (2017)). A yield function $\overline{y}_{pB}$ needs to be specified to complete the expression of w. It is chosen to be identical with the original breakage model (Einav, 2007b):

$$\overline{y}_{pB} = \left[\frac{\overline{E}_B}{\frac{\sqrt{E_B E_c}}{(1-B)\cos\omega}}\right]^2 + \left[\frac{\overline{p}}{\frac{p}{(1-B)\sin\omega}\sqrt{\frac{E_c}{E_B}}}\right]^2 + \left[\frac{\overline{q}}{Mp}\right]^2 - 1 = 0 \tag{5}$$

where ω is the coupling angle that controls the energy dissipation allocated to grain breakage and frictional sliding; M is the critical stress ratio; $\overline{p} = \overline{\sigma}_{ii}/3$ and $\overline{q} = \sqrt{\frac{3}{2}\left(\overline{\sigma}_{ij} - \overline{p}\delta_{ij}\right)\left(\overline{\sigma}_{ij} - \overline{p}\delta_{ij}\right)}$ are the mean and deviatoric stresses in dissipative space, respectively. Enforcing Ziegler's orthogonality condition in the form of $\overline{E}_B = E_B$ and $\overline{\sigma}_{ij} = \sigma_{ij}$, equation (5) becomes a teardrop-shaped yield surface in true stress space that can simultaneously account for shear- and compression-induced yielding of granular soils, which well

represents the yielding data of typical rockfill materials (Alonso et al., 2016). Finally, the inelastic evolution laws are derived according to the definition of flow potential (Houlsby, 2014):

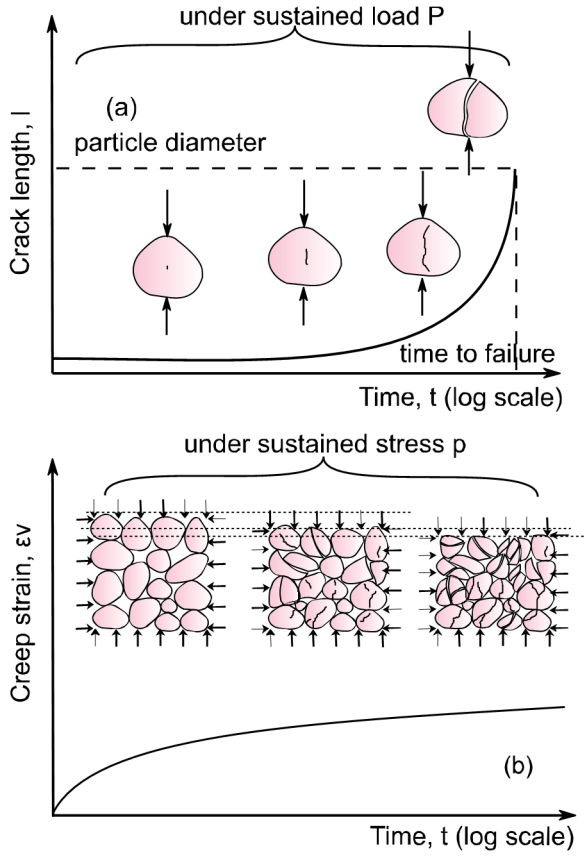

Figure 1: Schematic of (a) crack growth in particle (b) creep in a granular assembly (after Zhang and Buscarnera, 2017)

$$\dot{B} = \frac{\partial w}{\partial \overline{E}_B} = \dot{B}_0 \cos^2 \omega \varsigma_{pB}^{n/2} \tag{6}$$

$$\dot{\varepsilon}_{ij}^{p} = \frac{\partial w}{\partial \overline{p}} \frac{\partial \overline{p}}{\partial \overline{\sigma}_{ij}} + \frac{\partial w}{\partial \overline{q}} \frac{\partial \overline{q}}{\partial \overline{\sigma}_{ij}} = \frac{E_B \dot{B}_0}{p} \sin^2 \omega \varsigma_{pB}^{n/2} \left(\frac{\delta_{ij}}{3} \right) + \frac{E_c \dot{B}_0}{(1-B)^2} \frac{q}{M^2 p^2} \varsigma_{pB}^{n/2} \left(\frac{3}{2} \frac{s_{ij}}{q} \right) \tag{7}$$

where

$$\varsigma_{pB}\left(E_B, \sigma_{ij}\right) = \left\langle y_{pB}\left(E_B, \sigma_{ij}\right) \right\rangle = \left\langle \frac{(1-B)^2 E_B}{E_c} + \left(\frac{q}{Mp} \right)^2 - 1 \right\rangle \tag{8}$$

and $s_{ij} = \sigma_{ij} - p\delta_{ij}$ is the stress deviator; superscript 'p' denotes the plastic component. In summary, the model contains 8 parameters that characterize the elastic, plastic, breakage and rate-dependent behaviour of rockfills. All of them can be calibrated from standard laboratory programs: The elastic modulus K and G can be determined from the elastic portion of the stress-strain curves; the critical stress ratio M (or equivalently the critical-state friction angle) can be measured by shearing the specimen to failure; the grading index ϑ reflects relative distance between the initial GSD and the ultimate fractal GSD of the material; the coupling angle ω can be determined by matching the hardening portion of the stress-strain curves; the critical breakage energy E_c governs the size of the yield envelop and can be determined from the yielding stresses; the fluidity parameter $\dot{B}_0$ can be calibrated from creep tests; the corrosion index n can be inferred from the mineralogy of the rock or determined from the slope of the creep curves. More detailed calibration procedure is discussed in Section 5 with reference to the Shuibuya rockfill data.

Physically, $\dot{B}_0$ plays a similar role as fluidity in rheology as higher values of $\dot{B}_0$ promotes larger inelastic flow (equation (6)-(7)). n alters the nonlinearity of such rate-dependence which is a parameter inspired from subcritical fracture propagation analysis at grain scale (Zhang and Buscarnera, 2017). Figure 2a and b present the development of creep strain at vertical stress 10 MPa with various preloading rates. It can be observed that $\dot{B}_0$ controls the magnitude of the creep strain, while n controls the rate at which such creep strain develops and thus the shape of the creep curves. Figure 2c and d show the effect of critical breakage energy E_c on the compression and creep behaviours. One can see that E_c not only controls the size of the yield surface but also affects the amplitude of creep strain at prescribed stress levels. This is because smaller yield surface creates a higher overstress for a given stress state and thus drives more viscoplastic straining. This feature allows the long-term behaviours of rockfill dependent on its short-term properties, which is consistent with the findings in Oldecop and Alonso (2007).

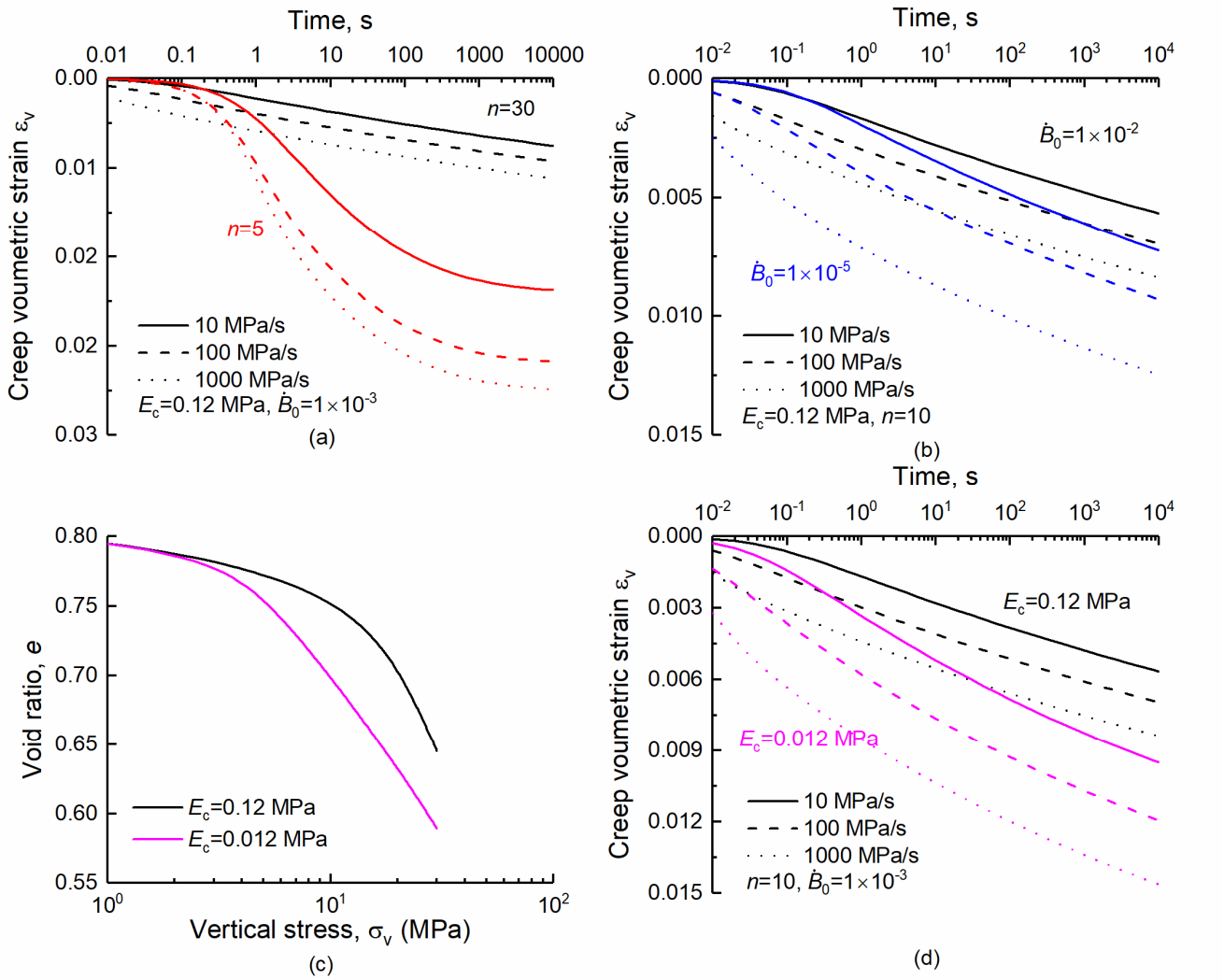

Figure 2: Effects of n, $\dot{B}_0$ and E_c on the simulated creep and compression responses using Virginia Beach sand parameters under oedometer compression condition. All the creep curves are obtained under σ_v=10MPa. The preloading rates at which such stress is achieved are given in the legends.

2.2 Scaling law

Rockfills consisting of larger grains exhibit smaller yield envelopes (Marsal, 1967; Marachi et al., 1972), lower apparent elastic modulus (Ramon et al., 2008; Zhou et al., 2016) and higher percentage of particle breakage when loaded to the same stress state (Varadarajan et al., 2003). These features are rooted in the size-dependent fracture strength of rock aggregates (Tapias et al., 2015; Ovalle et al., 2014). Zhang et al. (2016) have developed and validated the following relation to connect the particle fracture energy E_{pc} (i.e. an index reflecting the geometry and fracture toughness of the particle) with the critical breakage energy E_c (i.e. a parameter controlling the crushing resistance of the granular continuum):

$$E_c = (1-\phi)\,\xi E_{pc} \tag{9}$$

where ξ is an upscaling coefficient and ϕ is the initial porosity of the specimen. Such proposition is again motivated from the micro-macro analogy of the energy storage in particles at the onset of crushing, and the energy input to trigger distributed grain crushing in the assembly. The parameter ξ encapsulates all the factors that affect such upscaling process including the distribution of force chains, the packing and gradation of the specimen, and the angularity of soil particles. The value of ξ ranges between 0.1~0.4 with an average value of 0.25 (Sohn et al., 2017; Cil and Buscarnera, 2016). Using equation (9), grain-scale features such as particle diameter, angularity, the elastic and fracture properties can now enter the macroscopic description of granular assemblies. The analytical expressions of E_{pc} have been derived using linear elastic fracture mechanics (LEFM) and Weibull theory by assuming a variety of failure patterns (i.e. contact damage, central splitting, and randomly distributed cracks) and contact models (i.e. Hertzian, conical and flat contact). In general, particle fracture energy scales with grain size d_p through a power law relation:

$$E_{pc} \propto d_p^{-\lambda} \tag{10}$$

where λ is the scaling coefficient that depends on the failure and contact modes (Table 2). Combining equations (9) and (10), a useful scaling relation for E_c can be obtained:

$$E_{c,field} = E_{c,lab}\left(\frac{D_{50,field}}{D_{50,lab}}\right)^{-\lambda} \tag{11}$$

where $E_{c,lab}$ and $D_{50,lab}$ are the critical breakage energy and the median grain size for the reduced specimen, respectively; $E_{c,field}$ and $D_{50,field}$ are those for the prototype rockfills. To apply equation (11), λ can be measured from $E_{c,lab}$ vs. $D_{50,lab}$ data from oedometer compression tests on specimens with different D_{50}. If such test is not available, λ can be estimated from the existing dataset or analytical solutions. Zhang and Buscarnera (2014) has calibrated E_c for a wide range of coarse-grained soils and found an average value of

λ = 0.826, which is consistent with LEFM solutions for sub-rounded particles (λ = 0.833) (Zhang et al., 2016) .

Table 2: Grain size dependency on the fracture energy of single particles due to different contact and failure models

$E_{pc} \propto d_p^{-\lambda}$	Central splitting	Contact damage	Randomly distributed cracking
Linear elasticity	1	N/A	$6/w^*$
Hertzian elasticity	0.833	2.5	$5/w$
Conical elasticity	0.75	N/A	$4.5/w$

* w is the Weibull modulus, a constant that reflects the variability of the particle strength.

2.3 Breakage mechanics-based settlement analysis of rockfill dams

We propose the workflow outlined in Figure 3 to integrate the above theoretical components into a unified framework for predicting the settlement of rockfill dams. A step-by-step guidance for applying this procedure will be discussed later together with the Shuibuya CFRD case study. It is worth mentioning that the current scaling procedure only applies to the parameter controlling the onset of grain breakage (i.e. the size of the yield surface) via E_c, with the assumption that the elastic and visco-plastic parameters are independent of grain size. The scaling effect on the elastic properties of granular soils is unclear at this stage (Wood and Maeda, 2008). The study by Salgado et., al (2000) showed that the stiffness of clean sand at fixed relative density and confining stress level could decrease by adding small amount of silts. On the other hand, for geometrically similar gradations (i.e. samples with similar coefficient of uniformity C_u but has different D_{50}), Nakata et al. (2001)'s study on silica sand showed that the elastic stiffness is barely affected for as much as 5 times of increase in D_{50}. In the small strain regime, Wichtmann and Triantafyllidis (2009) argued that shear modulus is independent of D_{50} based on their 163 resonant column tests on 25 quartz sands with different gradations. Regarding $\dot{B}_0$ and n, the influence of scaling on the viscous properties of rockfills is little known. Only a few creep experiments on rockfills have been reported in the literature (Oldecop and Alonso, 2002; Zhang et al., 2017) and none of them have focused on the grain size effect. Oldecop and Alonso (2007) suggested that the long-term deformation of rockfill is intimately linked to their short-term behaviours. This can be indeed captured through the scaling of E_c, as a smaller yield surface

creates a higher overstress for a given stress state and thus drives more viscoplastic straining (Figure 2c and d). Regarding the rest of the model parameters, Wood and Maeda (2008) found that gradation has negligible influence on the critical stress ratio M; The slight variations of the grading index ϑ and breakage-plastic coupling angle ω with respect to D_{50} are also negligible comparing to the changes in E_c (Zhang and Buscarnera, 2014). For above reasons, we consider equation (11) is sufficient to capture the first-order scaling effects that are relevant to the settlement analysis conducted in this study.

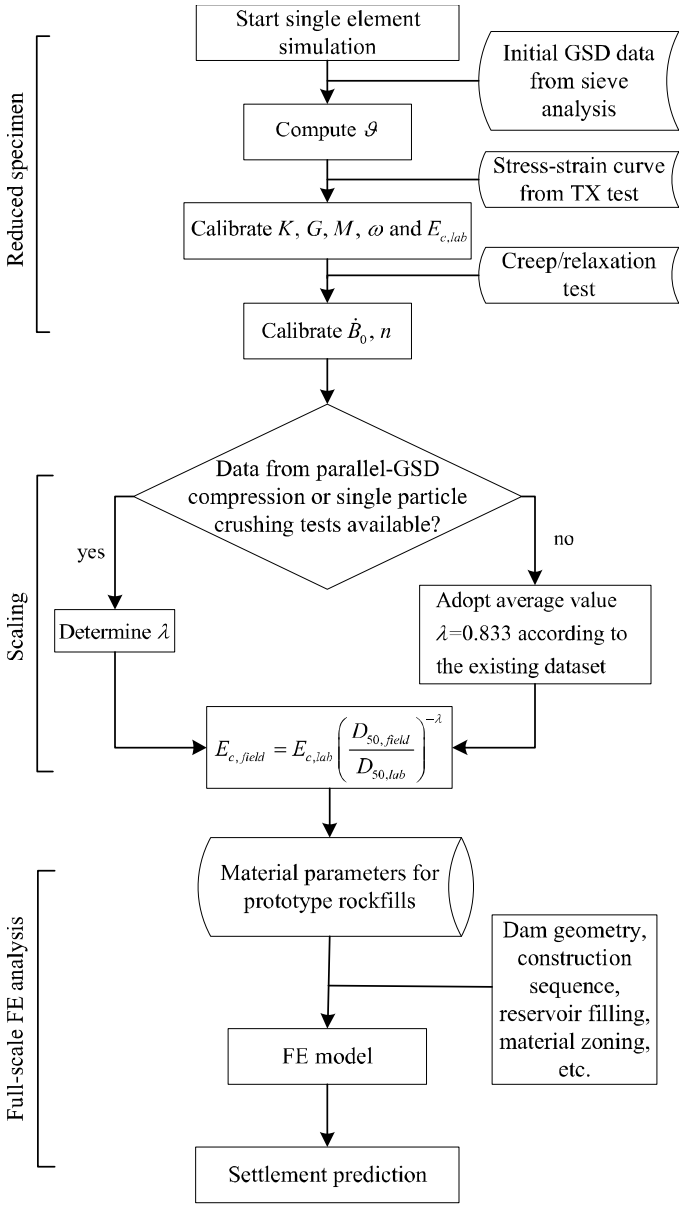

Figure 3: Flowchart of breakage-mechanics based settlement analysis of rockfill dams

3 THE SHUIBUYA CFRD

The Shuibuya CFRD is currently the tallest dam of its kind in the world, representing the state of the art of dam engineering and construction technology for rockfill structures. Data from element material testing to the global settlement is available through several technical papers and reports (Zhou et al., 2011a; Zhou et al., 2011b; Zhou et al., 2016), thus offering a unique opportunity to validate new rockfill models and analysing methodologies.

The Shuibuya dam was built on Qingjiang River in Badong City, Hubei Province, China (Figure 4a). It is 233.2 m high and 675 m long across a U-shaped river valley (Figure 4b). The maximum reservoir elevation is 400 m, with a water storage capacity of 4.59×10^9 m^3. The crest is 12 m wide installed with 5.2 m high L-shaped parapets. The slopes of both upstream and downstream dam are 1:1.4 (Figure 4c). The dam sits on a foundation at 175.8 m elevation, characterized by multiple strata of Longtan shale, Maokou limestone and Qixia limestone from top to bottom. The river wash is mainly sand gravel and also includes sandy boulder, sandy silt and silty clay phacoid. The typical zoning of the Shuibuya CFRD is shown in Figure 4c. It consists of: (1) 9.45×10^5 m^3 silty sandstone; (2) 5.5×10^4 m^3 clay; (3) 3.84×10^5 m^3 cushion material produced from Qixia limestone; (4) 7.21×10^5 m^3 transition material produced from excavated Qixia limestone; (5) 8.25×10^6 m^3 primary rockfill made of Maokou limestone; (6) 4.08×10^6 m^3 secondary rockfill made of the mixture of Qixia soft and hard limestone; (7) 2.22×10^6 m^3 downstream rockfill made of Qixia hard limestone and basalt. Laboratory tests have been conducted on reduced specimens of primary and secondary rockfills. Triaxial compression, proportional loading and constant mean stress tests have been performed under confining stresses from 0.2 MPa to 2.5 MPa. Creep tests have been also conducted for primary rockfills. The construction began in 2002 and completed in 2006, then the reservoir was gradually filled over the period of 10/2006 - 11/2008. The settlement monitoring system of the dam includes 18 reference stations, 56 external surface settlement markers (at the abutment, the face slab and the downstream shell of the dam), 70 internal displacement gauges distributed in three

representative cross sections (0+132 m, 0+212 m and 0+356 m). To monitor the settlement at dam crest, seven measurement points (SL1 to SL7) were installed along the dam longitudinal axis at the elevation of 405 m. Figure 5 shows the layout of 36 extensometers at the maximum cross-section (0+212) of the dam, a part of the internal settlement monitoring system (ISMS). The measured settlement together with the construction and filling records from 2004 to 2010 permits a comprehensive study on the deformation response of the dam subjected to combined gravity and hydrostatic loads.

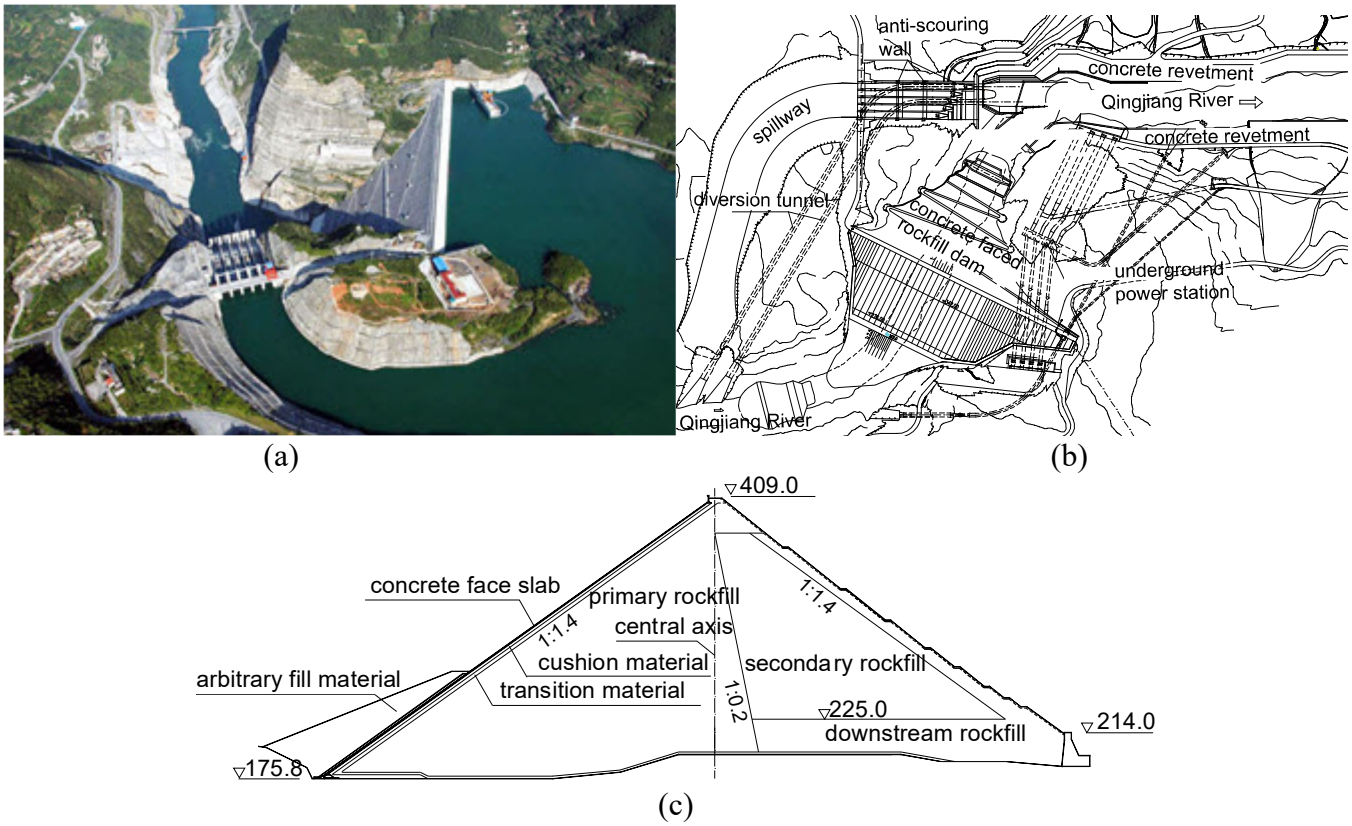

Figure 4: The (a) top view, (b) layout, and (c) zoning of the Shuibuya CFRD

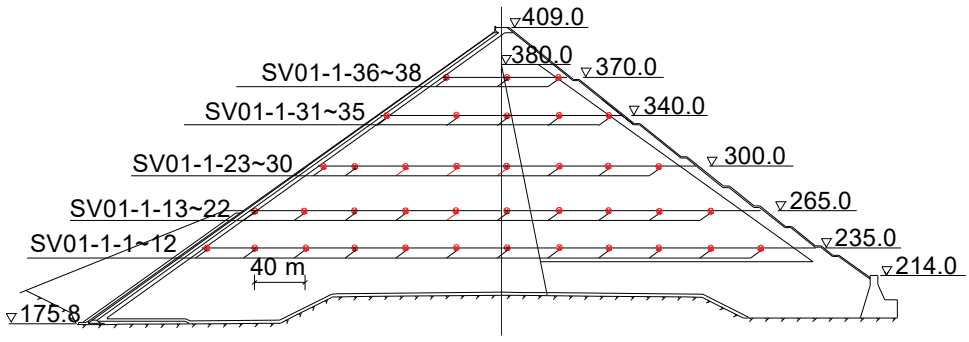

Figure 5: Layout of ISMS at the maximum cross-section (0+212 m) of the Shuibuya CFRD (The numbering of sensors increases from left to right).

4 UMAT IMPLEMENTATION AND FINITE ELEMENT MODEL

The rate-dependent breakage model is implemented in a user subroutine UMAT via an explicit error-controlled substepping algorithm adapted from Sloan (1987). A slight modification here is that Δt represents a finite increment in physical time instead of pseudo time that controls the loading progress for quasi-static models. Single-element tests are conducted to verify the implementation against a stand-along constitutive driver. Figure 6 compares the computed stress-strain curves and breakage evolution of drained triaxial compression tests under different strain rates using parameters calibrated for Virginia Beach sand. A perfect agreement between the two simulations is observed.

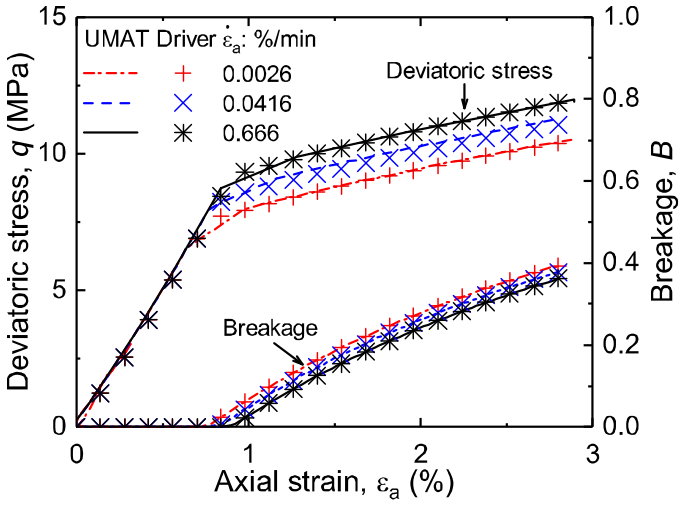

Figure 6: The predicted stress-strain and breakage curves of Virginia Beach sand from a stand-along constitutive driver and the implemented UMAT via single element simulation

Parameters for the primary and secondary rockfills of the Shuibuya dam are calibrated and scaled through the procedure depicted in Figure 3. Figure 7 reports the gradation of the reduced and prototype rockfills. The initial GSD of the reduced specimen is fitted by $F_0(x) = (x^{3-\beta} - D_{\min}^{3-\beta})/(D_{\max}^{3-\beta} - D_{\min}^{3-\beta})$ using β=2.36 and D_{min}=0.01 mm and D_{max} =60 mm. The ultimate fractal GSD is described by $F_u(x) = (x^{3-\alpha} - D_{\min}^{3-\alpha})/(D_{\max}^{3-\alpha} - D_{\min}^{3-\alpha})$ with the same values of D_{max} and D_{min}. Evidence from geological fault gouges (Sammis et al., 1987), high-pressure experiments (Hardin, 1985; Coop et al., 2004) and DEM simulations (Ben-Nun and Einav, 2010) showed that the ultimate fractal dimension α ranges between 2.6-2.7. In this study, $\alpha = 2.7$ is selected. Supplying the above coefficients in the expression of the grading index

(Einav, 2007a), a value of $\vartheta = 0.42$ is obtained. The mechanical parameters are calibrated through triaxial compression tests (Figure 8) which are conducted on fully saturated specimens with dry density 2.13 g/cm^3. Parameters K and G are obtained by matching the pre-yielding portion of the stress-strain curves; E_c, M and ω are determined according to the yielding and hardening responses. It is observed that the model well captures the stress-strain curves at different confining stresses, with some discrepancies on the volumetric response. This is due to the simple linear elasticity model adopted in this study and the lack of critical state concept in the current formulation of breakage mechanics. Improvements can be made by adopting pressure-dependent elasticity (Nguyen and Einav, 2009) and employing porosity as a state variable in the model (Tengattini et al., 2016), which may be pursued in advanced breakage-based simulations in the future.

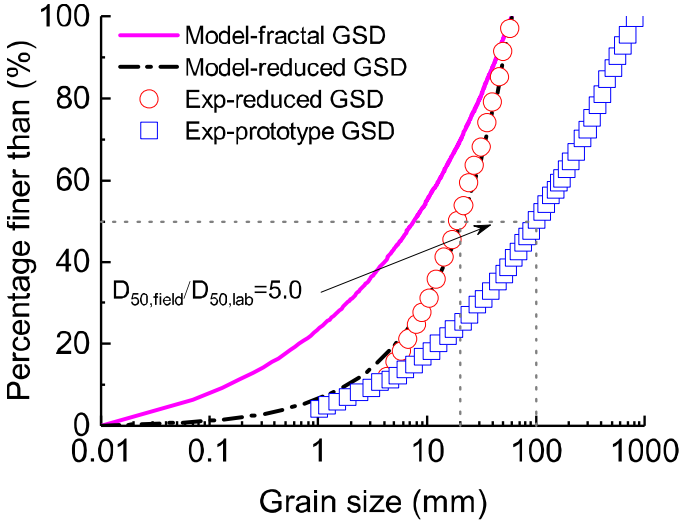

Figure 7: Grain size distribution of the reduced and the prototype rockfills and model calibration.

All the tests presented in Figure 8 were conducted under quasi-static condition (constant strain rate of 0.5%/min), thus cannot be used to calibrate the viscosity parameters. Instead, $\dot{B}_0$ and n are determined using data from the triaxial creep tests on the primary rockfill (Cheng and Ding, 2004)(Figure 9). Two sets of data are referenced here, differing in their confining stresses (2.7 MPa, 1.8 MPa) and the level of axial strains (6.2 %, 5.4 %) prior to the creep test. The obtained corrosion index n=6 is slightly lower than the typical range of n for quartz rocks (Atkinson, 1982) (meaning stronger rate sensitivity according to Figure 2a) due to the use of fully-saturated test condition and the water-sensitive nature of limestones. The same

viscous properties are assumed for the secondary rockfills for the lack of creep test data, considering a +-50% variation of $\dot{B}_0$ and n for the secondary rockfill has negligible effects on the simulation results based on our parametric analysis. Finally, the calibrated critical breakage energy $E_{c,lab}$ are upscaled to represent the crushability of the prototype rockfills. From Figure 7 it reads $D_{50,field} / D_{50,lab} = 5.0$. Substituting this value and the scaling parameter $\lambda = 0.833$ into equation (11), $E_{c,field}$ can be determined for the primary and secondary rockfills. Parameters determined through the above procedure are listed in Table 3. The downstream rockfill has very similar properties as the primary rockfill (Zhou et al., 2011b), thus is assigned with the same parameters. The cushion and the transition materials are expected to have minimum impact on the internal settlement given their small filling volume. Therefore, they are modelled by the Duncan-Chang E-B model with the same parameters reported in Zhou et al. (2011b).

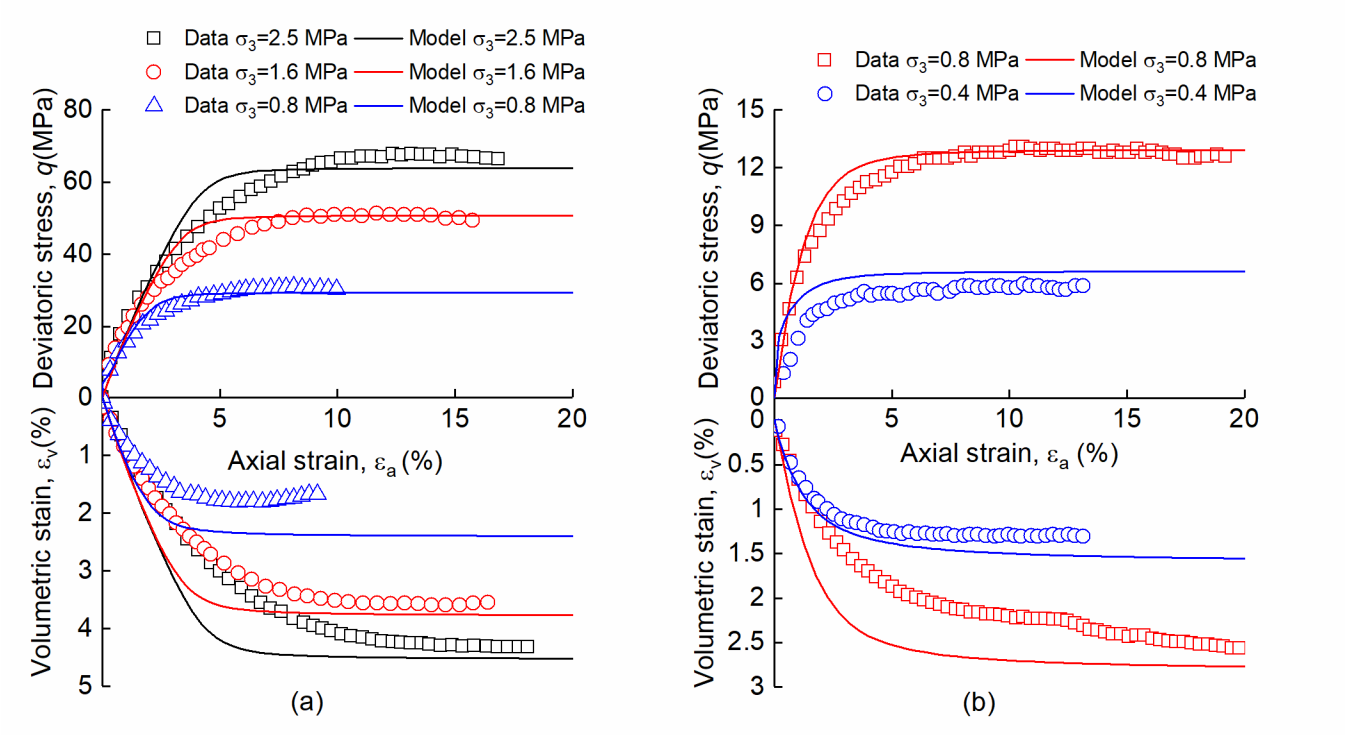

Figure 8: Model vs. data of triaxial tests on (a) primary rockfill and (b) secondary rockfill

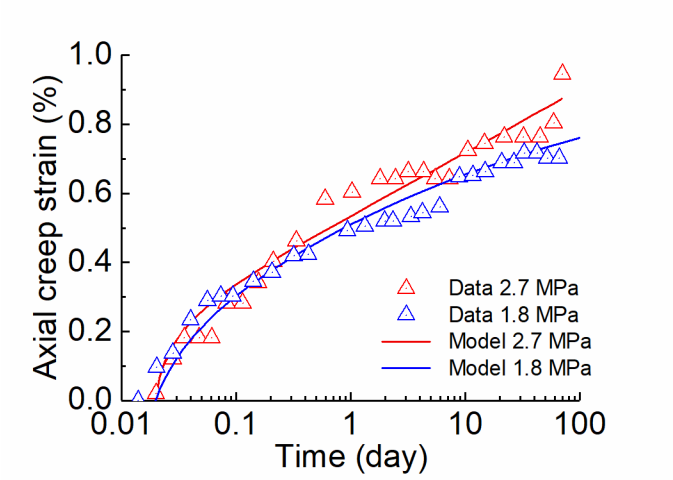

Figure 9: Creep curves of the primary rockfill of the Shuibuya CFRD. Data from Cheng and Ding (2004)

Table 3: Mechanical parameters for the primary, secondary and downstream rockfill of the Shuibuya CFRD

Definition of parameter	Symbol	Units	Primary rockfill/ downstream rockfill	Secondary rockfill
Grading index	ϑ		0.42	0.42
Bulk modulus	K	MPa	100	56
Shear modulus	G	MPa	150	80
Critical stress ratio	M		1.65	1.05
Breakage-plasticity coupling angle	ω	°	30	40
Reference breakage growth rate	$\dot{B}_0$	$1/s$	0.001	0.001
Corrosion index	n		6	6
Scaling coefficient	λ		0.833	0.833
Critical breakage energy for reduced specimens	$E_{c,lab}$	MPa	2.0×10^{-3}	1.8×10^{-3}
Critical breakage energy for prototype rockfill	$E_{c,field}$	MPa	5.2×10^{-4}	4.7×10^{-4}

Figure 10 presents the FE model for the Shuibuya dam considering the construction and impoundment sequence. The construction stage is simulated by 42 steps following exactly the construction timeline of the project. Simulation of these steps is realized by sequentially adding element sets and gradually increase the weight of each layer to achieve full gravitational load at the end of that construction period. An average density of 2150 kg/m^3 is assigned to the rockfills. Since the duration of each ramp loading is consistent with

the reported construction progress, the onset of creep is automatically determined by the constitutive model under realistic construction stress paths. The hydrostatic load is discretized and applied on the upstream surface in 58 steps in accordance with the reservoir level records to reflect the impact of impoundment and water level fluctuation during 2006~2010. The interfaces jointing the dam and the adjacent valleys and the bedrocks are prescribed as fixed displacement boundaries. The final three-dimensional FE model contains 11958 eight-node elements, 100 loading steps and 5 rockfill materials. It is worth mentioning that the moisture-sensitive behaviour of rockfills is not considered in the current model. The water level on the upstream and downstream side of the dam is quite steady and no extreme rainfall events or sudden raise of the water level has occurred during the operation of the dam. Therefore, this study has handled the water weakening effect in an intrinsic manner by calibrating the model against test results from saturated rockfill specimens (Figure 8). This permits a first-order mechanical analysis before taking complex environmental factors into consideration. Moisture effect has been recently incorporated in the breakage mechanics theory (Zhang and Buscarnera, 2018), which will be integrated with the proposed workflow for the future studies of rockfill dams under fluctuating hydrological conditions.

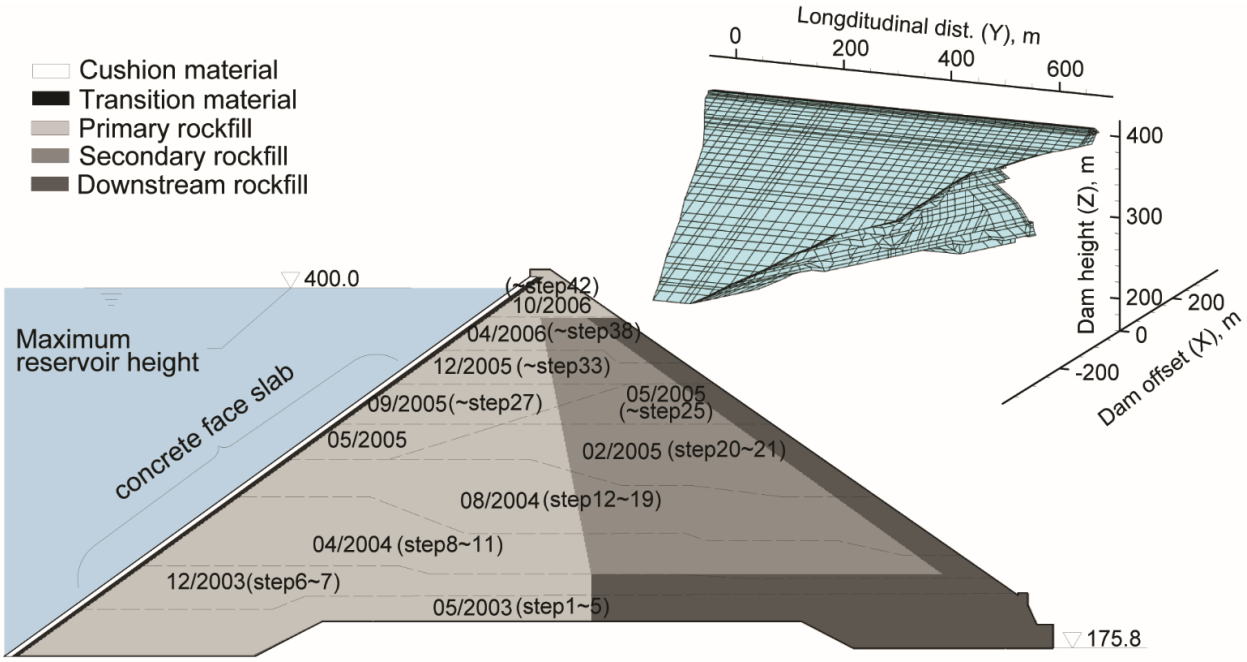

Figure 10: FE mesh of the Shuibuya CFRD

5 PREDICTION RESULTS

The predicted results from the FE analysis and the settlement data from the ISMS system are compared via two types of plot. The first type compares the settlement histories at different locations with those extracted from the output database of the FE simulation, highlighting the temporal evolution of deformation in responding to loading sequences. The second type compares the settlement contours at different time points, visualizing the spatial pattern of deformation within the dam.

5.1 Settlement history plots

The settlement observed at the dam crest reflects the accumulated compression of the dam body since the completion of construction (Gikas and Sakellariou, 2008). It is a good indicator of the differential settlement along the dam length and is important for structural integrity evaluations. Figures 11a and c present the recorded settlement history and distribution from seven surface markers on the dam crest, and Figures 11b and d report the predicted results from the FE analysis.

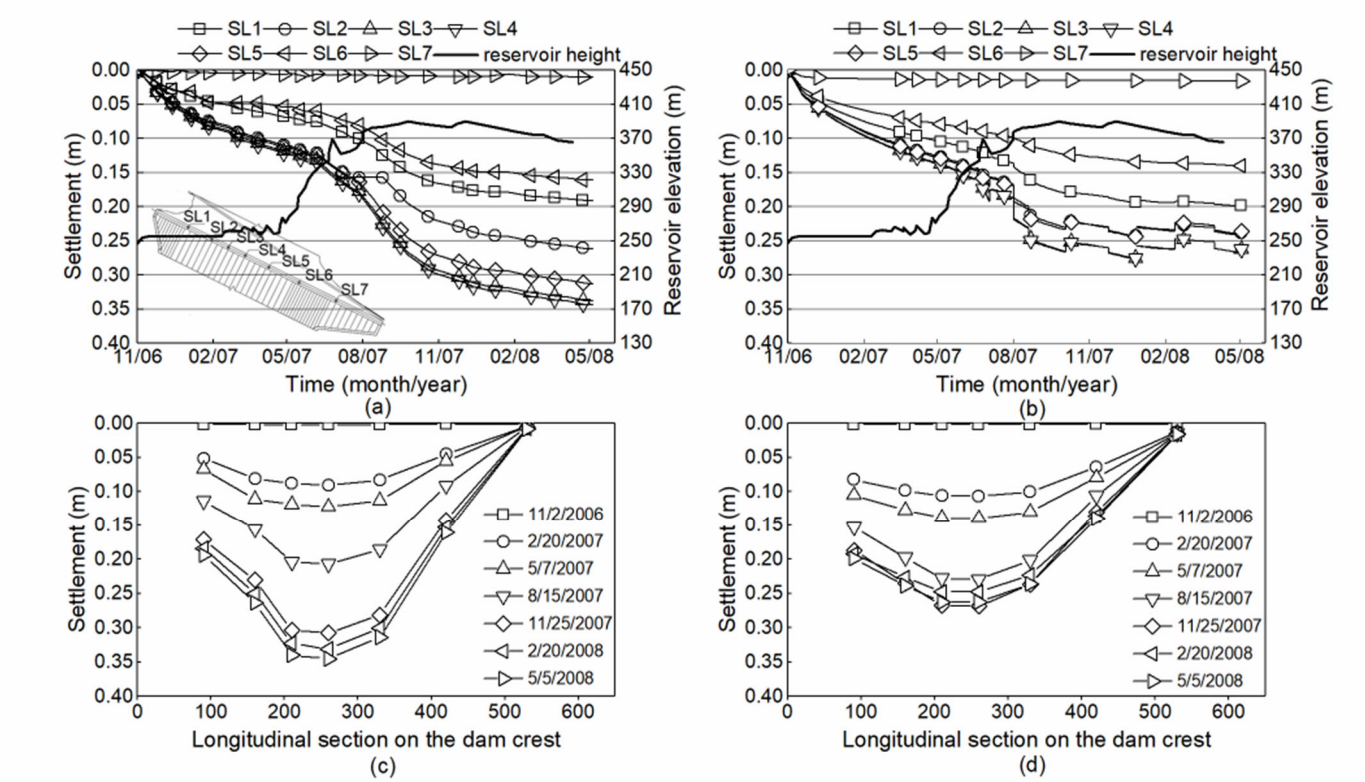

Figure 11: The measured (a) settlement history and (c) settlement profile along the dam crest from 11/2006 to 05/2008. (b) and (d) are the corresponding predictions from the FE analysis

Comparing Figures 11a and b, it is observed that the predicted crest settlement agrees well with monitoring data prior to the full impoundment on 08/2007. Upon reaching the maximum reservoir level, the computed settlement curves begin to oscillate and result an underestimated overall crest settlement. These oscillations are associated with the recovery of elastic stain caused by the partial release of the reservoir after peak storage and seasonal fluctuations of the reservoir level. For this reason, the accumulated creep strain under sustained water loading is offset by elastic rebounding, leading to the approximately constant crest settlement after 08/2007. This may be explained by the lack of plastic deformation mechanisms associated with cyclic loading paths. The upstream rockfills near the top of the dam have relatively low overburden stress, thus fluctuation of the reservoir level will induce large magnitude of loading cycles that can plastically compact the rockfills. Modelling this behaviour requires the extension of breakage models with hypoplasticity features as recently discussed by Einav (2012) and Das and Bajpai (2017). It is worth noting that the effect of cyclic degradation is much less important for rockfills at greater depths in the dam, as the magnitudes of cyclic loading become negligible comparing to the overburden stresses. This will be soon confirmed by the lack of oscillations in the computed settlement curves inside the dam. The saddle-shape settlement profile across the crest shown in Figure 11c is successfully captured by the FE analysis (Figure 11d). The predicted profiles before 08/2007 agrees particularly well with the measured ones, suggesting a good performance of the model in representing the monotonic behaviour of rockfills. Again, the overall crest settlement after 08/2007 is underpredicted due to the cyclic effect.

Among the three monitored cross sections, the 0+212m section is selected as the focus of comparisons as it is the maximum cross section of the dam and has installed more sensors than the other two. Figures 12a and b report the measured and predicted settlement histories at elevation of 235 m, respectively. Several characteristic trends are successfully captured by the FE model: (1) settlement near the centre of the dam (reported by SV01-1-6 to SV01-1-10) develops faster than that near the upstream concrete face (SV01-1-1 to SV01-1-5) during construction, while the trend is reversed during the impoundment stage; (2) settlement

continues to develop after the dam is filled to maximum capacity (08/2007). The first trend can be explained by the fact that the rockfills near the upstream surface is only subjected to a small portion of overburden pressures during construction, but serves as the main load-bearing material upon reservoir filling, thus responding more sensitively to impoundment. The second trend is mainly attributed to the creep behaviour of rockfill materials. Figures 13 presents the measured and predicted settlement for elevation 300 m. Again, the predicted maximum settlements at different elevations agree remarkably well with the recorded values. Such level of agreement is given by the forward procedure described in Figure 3 rather than from back analysis.

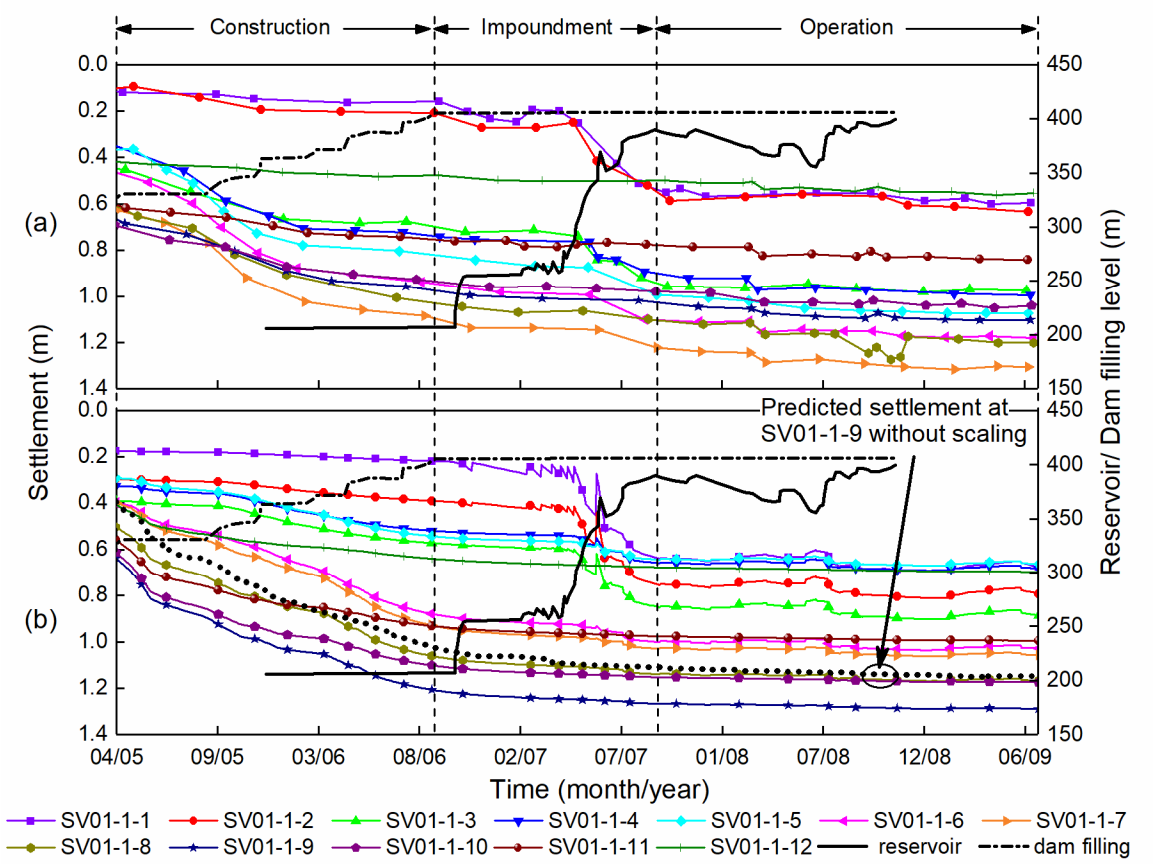

Figure 12: The (a) measured and (b) predicted settlement at the elevation of 235 m in the 0+212 m cross section

In the operation stage, slightly higher creep rates (0.05 m/ yr) are observed for monitoring points SV01-1-6 to SV01-1-8 than the computed ones (0.02 m/ yr). These points are located at the lowest elevation monitored (235m) near the central line of the dam. Noticing such high creep rates disappeared at higher

elevations (300 m, Figure 13), it is inferred that the accelerated creep is caused by possible seepage flow with low phreatic line near the dam foundation. This can cause high moisture content or even full saturation for rockfills at low elevations and accelerate their degradation. A fully coupled hydromechanical analysis with moisture-dependent breakage model may capture these subtle differences in the future studies. Another observation is that among the predicted settlement curves during the operation stage, those extracted at locations near the upstream surface of the dam (SV01-1-1 to SV01-1-5) exhibit similar fluctuations as to the crest settlement curves, while those near the centre of the dam (SV01-1-6 to SV01-1-10) are relatively insensitive to the fluctuation of reservoir level. This is consistent with the previous conclusion that the cyclic loading induced by changes of water level is less significant for internal rockfills away from the concrete slabs. The predicted maximum settlement at this elevation is in perfect agreement with the observed value

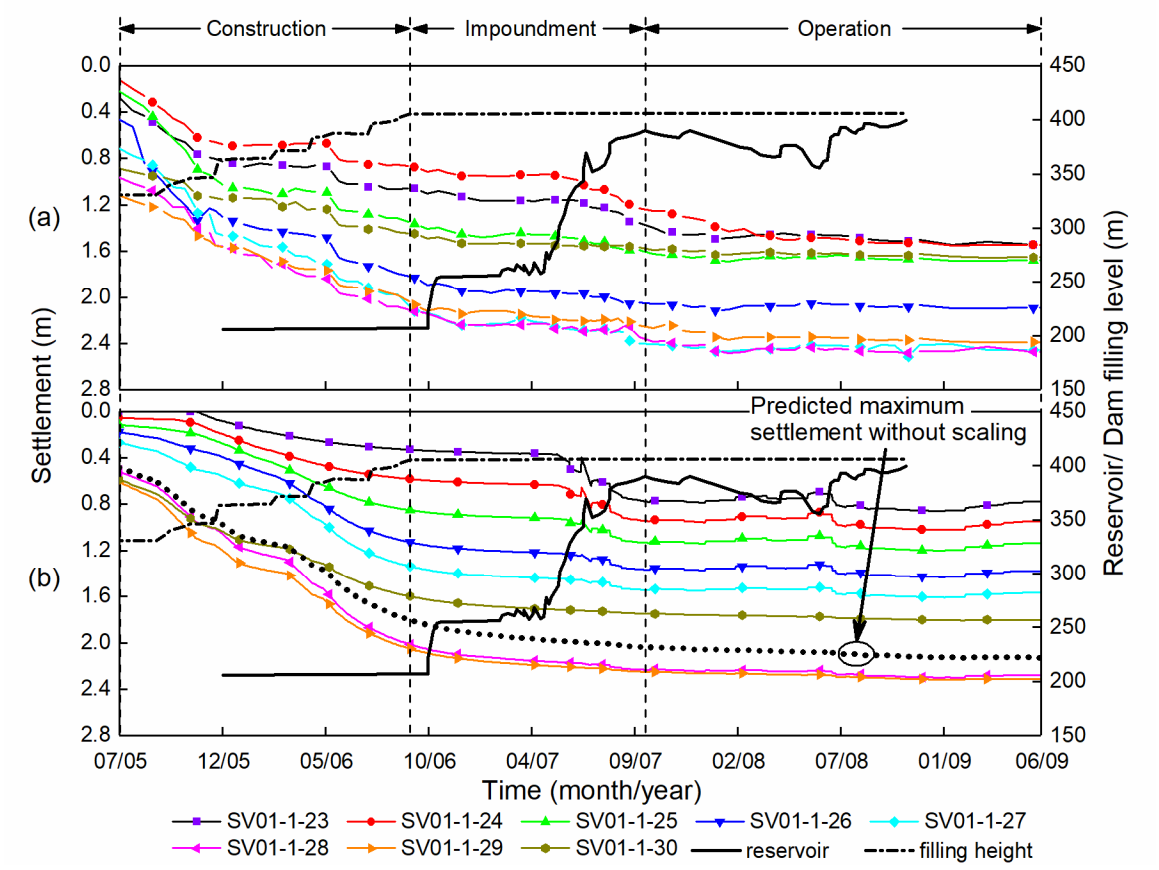

Figure 13: The (a) measured and (b) predicted settlement at the elevation of 300 m in the 0+212 m cross section

(1.3 m). However, such magnitude is predicted to occur at location SV01-1-9 instead of SV01-1-7 as shown in Figure 12a. This indicates a slight discrepancy on the predicted spatial distribution of settlements, which is more conveniently discussed using contour plots in the next section.

5.2 Settlement contour at different time points

Figure 14 reports the settlement contours for the 0+212 m section from the end of construction (Figure 14a) to the latest monitoring record (Figure 14d). For each plot, the contour on the left presents the data measured from the ISMS and that on the right presents the predictions of the FE model. The region beyond the coverage of ISMS instrumentation is left blank. In general, a satisfactory agreement is observed. The FE model successfully captured that the maximum settlement zone locates near the downstream side of the dam, given the relatively low strength and stiffness of the secondary rockfill. The predicted contours locate slightly to the right of the measured ones, which explains the mismatch on the sensors reporting the maximum settlement discussed in the previous section. The maximum settlement increased from 2.2 m to 2.45 m over 4 years of operation, which is also captured by the FE model. All the contours from FE simulations contain some rough edges. They are caused by the discretization of the construction steps and consequently different total time allowed for each rockfill layers to develop creep strains. In summary, these agreements support the predictive capability of the proposed constitutive model and the upscaling strategy for the settlement assessment of large rockfill structures.

6 DISCUSSIONS

6.1 Grain size effect

A separate FE simulation is conducted using unscaled parameters (i.e. $E_{c,lab}$ instead of $E_{c,field}$). The predicted maximum settlement at elevations 235m and 300m are plotted together with the baseline results in Figures 12b and 13b, respectively. Figure 15 reports the computed settlement contour in 04/2010 using both scaled (black solid lines) and unscaled (red dash dotted lines) value of E_c. As expected, the use of $E_{c,lab}$ would

substantially underestimate the overall settlement by an average of 14%. This implies that neglecting the scaling effect in large CFRDs can promote unconservative designs of the concrete slabs and crest highways.

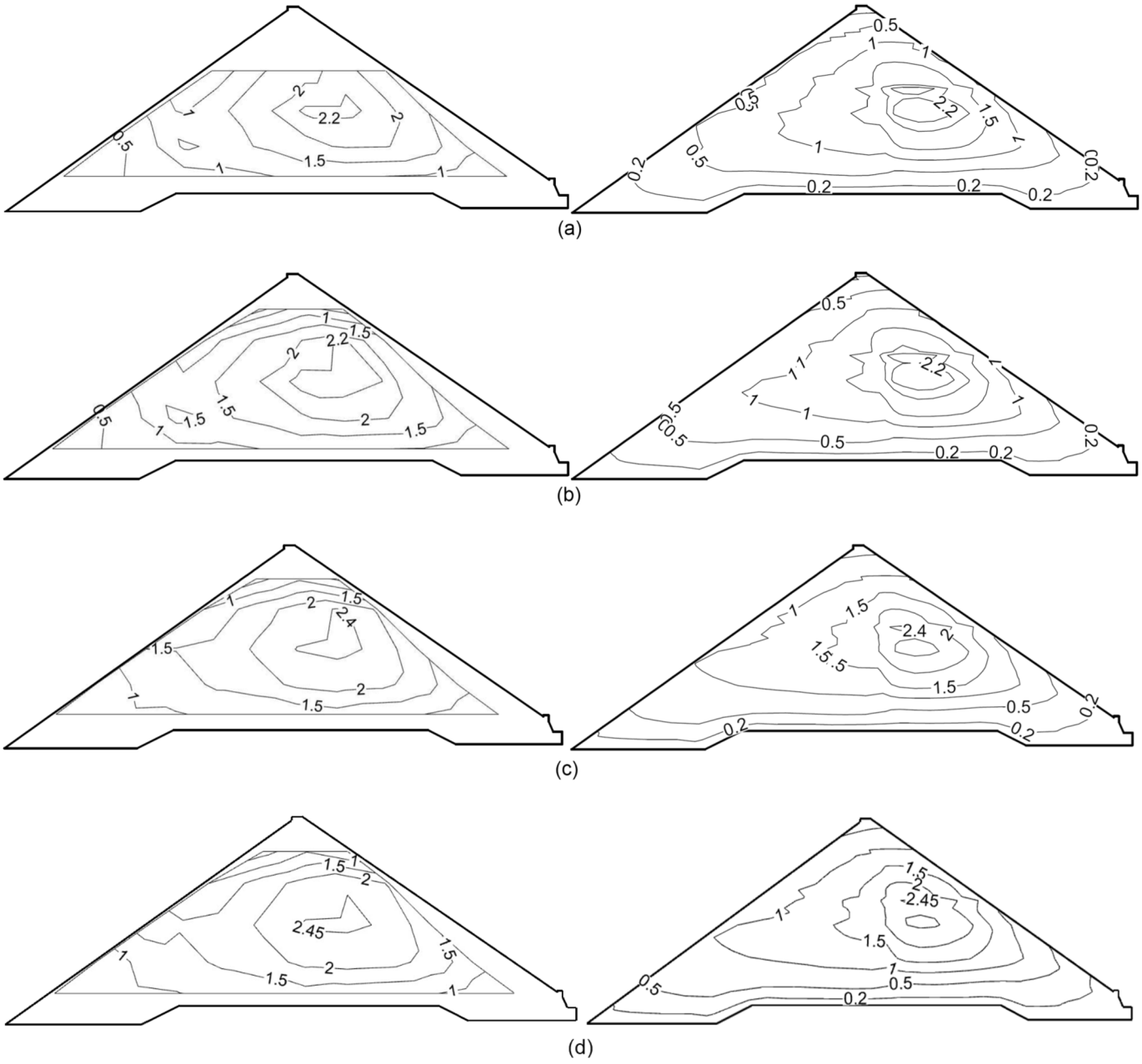

Figure 14: Measured vs. predicted settlement at the 0+212 m cross section in (a) 12/2006; (b) 07/2007; (c) 11/2008; (d) 04/2010

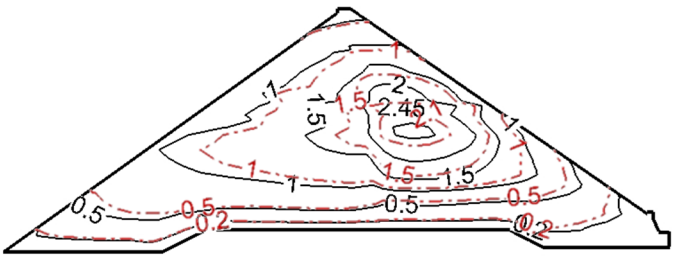

Figure 15: Grain size effect on the predicted settlement contour at the 0+212 m cross section in 04/2010

6.2 Time effect

The contribution of creep on the total deformation can be separated by turning off the rate-dependent feature of the model. This can be achieved by increasing the value of either n or $\dot{B}_0$, i.e. to create instantaneous inelastic flow even under small overstress according to equations (6) and (7). It is found that the use of n = 50 is sufficient to supress the time effect in this study. The predicted settlement histories and contours are shown in Figures 16 and 17. Comparing Figure 16 with Figure 13a, it is observed that the settlement develops quite similarly at the construction stage, but diverts during the impoundment and the operation

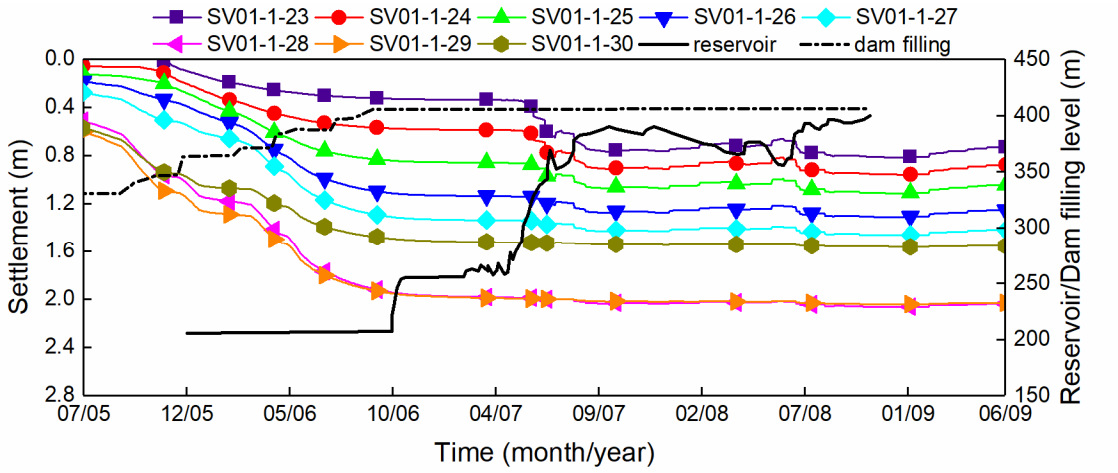

Figure 16: Predicted settlement without creep at the 0+212 m cross section on elevation of 300 m

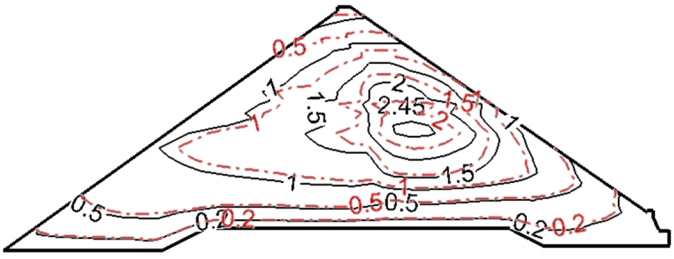

Figure 17: Time effect on the predicted settlement contour at the 0+212 m cross section in 04/2010

phases. Particularly, settlement is almost ceased after the maximum reservoir level is reached according to this simulation. The predicted maximum settlement 2.0 m is 18% lower than the field observations. In comparison to the settlement contours with creep (black solid lines in Figure 17), the predictions without creep (red dash dotted lines) will underestimate the maximum settlement as well as alter the global deformation pattern. For example, the settlement level near the centre of the dam is significantly reduced while near the boundary of the dam is not much affected.

6.3 Breakage evolution

A unique feature of breakage mechanics-based deformation analysis is to track the microstructural degradation of rockfills at any spatial and temporal points via the breakage index B. Figures 18a and b report the predicted breakage contours immediately after construction and after three years of operation. It is obvious that rockfills located at the lower part near the centre of the dam experience the most severe breakage due to the self-weight of the dam. Less breakage is predicted for rockfills near the faces and the crest of the dam. Over three years of operation, the breakage contours are expanded, governed by the delayed breakage evolution law (6). It is believed, however, that the overall magnitude of the breakage index inside the dam is over predicted. A value of B=0.9 suggests that the rockfill is almost completely crushed to its ultimate fractal state, which is not likely for the stress levels encountered in this dam (0.8-2.4 MPa). Such overprediction is due to the idealized breakage evolution law in the current model. Under isotropic compression, this law can be written as:

$$E_B = \frac{E_c}{(1-B)^2} \tag{12}$$

, through which a B-p relation can be obtained by substituting equation (4) and replace ε_v with p using elastic relation. Figure 19 plots this relation extracted from a lower central node in the FE model together with the experimental data from Pyramid dam rockfills (Yin et al., 2016). Apparently, the predicted B evolves

towards unity at a rate that is much faster as compared to experimental measurements. This points out a need for developing more accurate and flexible breakage evolution law for breakage models.

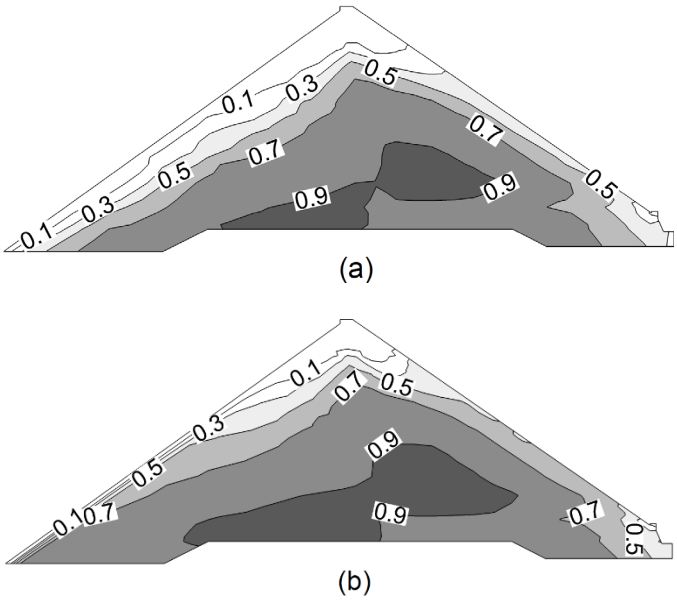

Figure 18: Breakage contour of Shuibuya CFRD in (a) 10/2006; (b) 04/2010

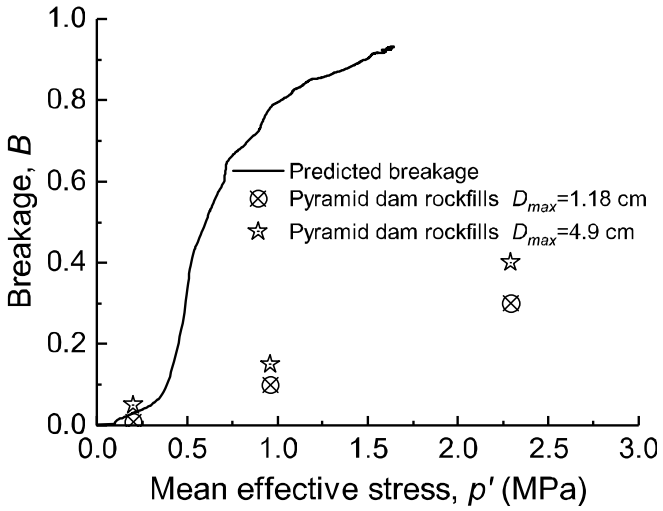

Figure 19: Predicted breakage evolution near the centre of Shuibuya dam and measured breakage values for Pyramid dam rockfill triaxial sheared to critical state (data from Yin et al. (2016))

7 CONCLUSION

We proposed a procedure for the settlement analysis of rockfill dams that can account for the time- and scale- dependent behaviours of rockfills. The new methodology integrates the rate-dependent breakage mechanics theory and the scaling law for the critical breakage energy of the granular matrix. The procedure

requires 8 model parameters and 1 scaling parameter which can be readily calibrated from standard laboratory testing programs. The predictive performance of this framework is validated through a comprehensive case study on the Shuibuya CFRD. The main observations are: (1) the spatial distribution and temporal evolution of the settlement of the dam are well captured by the model using scaled parameters; (2) disabling the scaling and the time-dependent features of the model will result in an average of 14% and 18% underprediction of the dam settlement, respectively. These findings suggest that the incorporation of grain breakage and the associated microscale processes is the key step towards improved deformation predictions of rockfill structures. Comparing to the usual E-B model-based FE analysis, the proposed method has the following advantages: (1) the extrapolation of test results from reduced specimens to the properties of prototype rockfills can be performed on a rational basis using analytical tools developed from particle scale mechanics; (2) the model tracks the evolution of the grain size distribution during the course of loading process, allowing for explicit modelling of the time and scale effect associated with grain fracturing; (3) the model parameters have clear physical meanings and straightforward calibration procedures, thus can be easily implemented for practical applications. The proposed framework is susceptible to numerous generalizations and enhancements. Relative humidity can be introduced as an additional degree of freedom in the FE analysis in combination with a moisture-dependent breakage model (e.g. Zhang and Buscarnera (2018)). This is necessary for applications involving strong coupling with hydrological condition such as clay core rockfill dams (CCRDs). Cyclic degradation can be modelled by introducing dissipation mechanisms within the yield surface (e.g. Das and Bajpai (2017)), which allows for more accurate description of rockfills near the upstream. Finally, the current model overpredicts the extent of breakage inside the dam, calling for a more accurate evolution laws specific for rockfill materials. In summary, this study sets an important first step towards a fully-coupled hydromechanical framework for deformation analysis of rockfill structures, taking into account the effects of loading cycles, flooding, rainfall infiltration, particle breakage, creep and grain size scaling.

8 ACKNOWLEDGEMENT

This work was supported by funds from the University of Colorado Boulder, Department of Civil, Environmental, and Architectural Engineering.

REFERENCE

Alonso, E., Olivella, S., Soriano, A., Pinyol, N. & Esteban, F. (2011) Modelling the response of Lechago earth and rockfill dam. *Géotechnique* **61(5)**:387-407.

Alonso, E. E., Romero, E. E. & Ortega, E. (2016) Yielding of rockfill in relative humidity-controlled triaxial experiments. *Acta Geotechnica* **11(3)**:455-477.

Atkinson, B. K. (1982) Subcritical crack propagation in rocks: theory, experimental results and applications. *Journal of Structural Geology* **4(1)**:41-56.

Ben-Nun, O. & Einav, I. (2010) The role of self-organization during confined comminution of granular materials. *Philosophical Transactions of the Royal Society of London A: Mathematical, Physical and Engineering Sciences* **368(1910)**:231-247.

Chávez, C., Romero, E. & Alonso, E. (2009) A rockfill triaxial cell with suction control.

Cheng, Z.-L. & Ding, H.-S. (2004) Creep test for rockfill. *CHINESE JOURNAL OF GEOTECHNICAL ENGINEERING-CHINESE EDITION-* **26**:473-476.

Cil, M. B. & Buscarnera, G. (2016) DEM assessment of scaling laws capturing the grain size dependence of yielding in granular soils. *Granular Matter* **18(3)**:36.

Collins, I. & Houlsby, G. (1997) Application of thermomechanical principles to the modelling of geotechnical materials. *Proceedings of the Royal Society of London A: Mathematical, Physical and Engineering Sciences* **453(1964)**:1975-2001.

Coop, M., Sorensen, K., Freitas, T. B. & Georgoutsos, G. (2004) Particle breakage during shearing of a carbonate sand. *Géotechnique* **54(3)**:157-164.

Das, A. & Bajpai, P. K. (2017) A hypo-plastic approach for evaluating railway ballast degradation. *Acta Geotechnica*:1-18.

Einav, I. (2007a) Breakage mechanics-part I: theory. *Journal of the Mechanics and Physics of Solids* **55(6)**:1274-1297.

Einav, I. (2007b) Breakage mechanics-Part II: Modelling granular materials. *Journal of the Mechanics and Physics of Solids* **55(6)**:1298-1320.

Einav, I. (2012) The unification of hypo-plastic and elasto-plastic theories. *International Journal of Solids and Structures* **49(11)**:1305-1315.

Gikas, V. & Sakellariou, M. (2008) Settlement analysis of the Mornos earth dam (Greece): Evidence from numerical modeling and geodetic monitoring. *Engineering Structures* **30(11)**:3074-3081.

Hardin, B. O. (1985) Crushing of soil particles. *Journal of Geotechnical Engineering* **111(10)**:1177-1192.

Houlsby, G. T. (2014) Dissipation rate functions, Pseudopotentials, Potentials and Yield Surfaces. In *Beyond the Second Law*.) Springer, pp. 73-95.

Houlsby, G. T. & Puzrin, A. M. (2007) *Principles of hyperplasticity: an approach to plasticity theory based on thermodynamic principles.* Springer Science & Business Media.

Marachi, N. D., Chan, C. K. & Seed, H. B. (1972) Evaluation of properties of rockfill materials. *Journal of Soil Mechanics & Foundations Div* **98(SM1)**:95-114.

Marsal, R. J. (1967) Large-scale testing of rockfill materials. *Journal of the Soil Mechanics and Foundations Division* **93(2)**:27-43.

Marsal, R. J. (1973) Mechanical properties of rockfill. *Publication of: Wiley (John) and Sons, Incorporated.*

Naylor, D., Maranha Das Neves, E., Mattar, D. & Veiga Pinto, A. (1986) Prediction of construction performance of Beliche Dam. *Géotechnique* **36(3)**:359-376.
Nguyen, G. D. & Einav, I. (2009) The energetics of cataclasis based on breakage mechanics. *Pure and Applied Geophysics* **166**:1693-1724.
Oldecop, L. & Alonso, E. (2002) Fundamentals of rockfill time-dependent behaviour. *Unsaturated Soils, Juca, de Campos & Marinho (eds)*:793-798.
Oldecop, L. A. & Alonso, E. (2007) Theoretical investigation of the time-dependent behaviour of rockfill. *Géotechnique* **57(3)**:289-301.
Ovalle, C., Frossard, E., Dano, C., Hu, W., Maiolino, S. & Hicher, P.-Y. (2014) The effect of size on the strength of coarse rock aggregates and large rockfill samples through experimental data. *Acta Mechanica* **225(8)**:2199.
Pramthawee, P., Jongpradist, P. & Sukkarak, R. (2017) Integration of creep into a modified hardening soil model for time-dependent analysis of a high rockfill dam. *Computers and Geotechnics* **91**:104-116.
Ramon, A., Alonso, E. & Romero, E. (2008) Grain size effects on rockfill constitutive behaviour. In *Proceedings of the 1st European conference on unsaturated soils. Taylor & Francis*.), pp. 341-347.
Sammis, C., King, G. & Biegel, R. (1987) The kinematics of gouge deformation. *Pure and Applied Geophysics* **125(5)**:777-812.
Sloan, S. W. (1987) Substepping schemes for the numerical integration of elastoplastic stress–strain relations. *International Journal for Numerical Methods in Engineering* **24(5)**:893-911.
Sohn, C., Zhang, Y. D., Cil, M. & Buscarnera, G. (2017) Experimental assessment of continuum breakage models accounting for mechanical interactions at particle contacts. *Granular Matter*:In press.
Tapias, M., Alonso, E. & Gili, J. (2015) A particle model for rockfill behaviour. *Géotechnique* **65(12)**:975-994.
Tengattini, A., Das, A. & Einav, I. (2016) A constitutive modelling framework predicting critical state in sand undergoing crushing and dilation. *Géotechnique* **66(9)**:695-710.
Varadarajan, A., Sharma, K., Venkatachalam, K. & Gupta, A. (2003) Testing and modeling two rockfill materials. *Journal of Geotechnical and Geoenvironmental Engineering* **129(3)**:206-218.
Wen, L., Chai, J., Xu, Z., Qin, Y. & Li, Y. (2017) Monitoring and numerical analysis of behaviour of Miaojiaba concrete-face rockfill dam built on river gravel foundation in China. *Computers and Geotechnics* **85**:230-248.
Wood, D. M. & Maeda, K. (2008) Changing grading of soil: effect on critical states. *Acta Geotechnica* **3(1)**:3.
Yin, Z.-Y., Hicher, P.-Y., Dano, C. & Jin, Y.-F. (2016) Modeling mechanical behavior of very coarse granular materials. *Journal of engineering mechanics* **143(1)**:C4016006.
Zhang, B., Chen, T., Peng, C., Qian, X. & Jie, Y. (2017) Experimental Study on Loading-Creep Coupling Effect in Rockfill Material. *International Journal of Geomechanics* **17(9)**:04017059.
Zhang, Y. & Buscarnera, G. (2017) A rate-dependent breakage model based on the kinetics of crack growth at the grain scale. *Géotechnique* **67(11)**:953-967.
Zhang, Y. & Buscarnera, G. (2018) Breakage mechanics for granular materials in surface-reactive environments. *Journal of the Mechanics and Physics of Solids* **112**:89-108.
Zhang, Y. D. & Buscarnera, G. (2014) Grainsize dependence of clastic yielding in unsaturated granular soils. *Granular Matter* **16(4)**:469-483.
Zhang, Y. D., Buscarnera, G. & Einav, I. (2016) Grainsize dependence of yielding in granular soils interpreted using fracture mechanics, breakage mechanics and Weibull statistics. *Géotechnique* **66(2)**:149-160.
Zhou, W., Chang, X., Zhou, C. & Liu, X. (2010) Creep analysis of high concrete-faced rockfill dam. *International Journal for Numerical Methods in Biomedical Engineering* **26(11)**:1477-1492.

Zhou, W., Hua, J., Chang, X., Yang, Q. & Ma, G. (2011a) Estimation of work status and deformation prediction of Shuibuya CFRD. *Chinese Journal of Geotechnical Engineering* **33**:65-70.
Zhou, W., Hua, J., Chang, X. & Zhou, C. (2011b) Settlement analysis of the Shuibuya concrete-face rockfill dam. *Computers and Geotechnics* **38(2)**:269-280.
Zhou, W., Li, S., Zhou, Z. & Chang, X. (2016) Remote sensing of deformation of a high concrete-faced rockfill dam using InSAR: A study of the Shuibuya dam, China. *Remote Sensing* **8(3)**:255.
Zhu, S., Liang, X.-P. & Feng, S.-R. (2009) Back analysis of mechanical parameters of naturally graded rockfill materials based on large-scale loading plate tests. *Chinese Journal of Geotechnical Engineering* **7**:030.